Available online at www.sciencedirect.com
SCIENCE DIRECT®
Physica D 202 (2005) 37–59
PHYSICA D
www.elsevier.com/locate/physd

Reduction of a model of an excitable cell to a one-dimensional map

Georgi S. Medvedev*

Department of Mathematics, Drexel University, 3141 Chestnut Street, Philadelphia, PA 19104, USA

Received 13 August 2004; received in revised form 5 January 2005; accepted 27 January 2005
Available online 3 March 2005
Communicated by C.K.R.T. Jones

Abstract

We use qualitative methods for singularly perturbed systems of differential equations and the principle of averaging to compute the first return map for the dynamics of a slow variable (calcium concentration) in the model of an excitable cell. The bifurcation structure of the system with continuous time endows the map with distinct features: it is a unimodal map with a boundary layer corresponding to the homoclinic bifurcation in the original model. This structure accounts for different periodic and aperiodic regimes and transitions between them. All parameters in the discrete system have biophysical meaning, which allows for precise interpretation of various dynamical patterns. Our results provide analytical explanation for the numerical studies reported previously.

Keywords: One-dimensional map; Singularly perturbed systems; Neurons

1. Introduction

Understanding mechanisms for patterns of electrical activity of neural cells (firing patterns) and principles for their selection and control is fundamental for determining how neurons function [10]. After a classical series of papers by Hodgkin and Huxley [18] nonlinear differential equations became the main framework for modeling neurons. The bifurcation theory for nonlinear ordinary differential equations [16,24] provides a powerful suite of tools for analyzing neuronal models. Many such models reside near multiple bifurcations. Consequently, in using bifurcation analysis one often encounters rich and complicated bifurcation structure. Therefore, it is desirable to distinguish the universal features pertinent to a given dynamical behavior from the artifacts peculiar to a particular model. This is important in view of the unavoidable simplifications one makes in the process of modeling such complex systems as neural cells, and under the conditions when many parameters are known approximately. The

* Tel.: +1 215 895 6612; fax: +1 215 895 1582.
E-mail address: medvedev@drexel.edu (G.S. Medvedev).

0167-2789/$ – see front matter © 2005 Elsevier B.V. All rights reserved.
doi:10.1016/j.physd.2005.01.021

goal of the present paper is to describe some general traits of the bifurcation structure of a class of models of bursting neurons. They follow from the generic properties of two-dimensional flows near a homoclinic bifurcation. We present a method of reduction of a model of an excitable cell to a one-dimensional map. The bifurcation structure of the system with continuous time endows the map with distinct features: it is a unimodal map with a boundary layer corresponding to the homoclinic bifurcation in the original model. The qualitative features of this map account for periodic and aperiodic regimes and transitions between them. Our analytical results are consistent with the numerical results reported in the literature [6,7], which, in turn, reflect many salient features of the experimental data. Our approach in this paper is to describe general features of the bifurcation structure of the problem: we do not pursue the study of the fine structure in the (small) parameter windows of complex and possibly chaotic dynamics. We believe that more detailed information in these windows in the parameter space can be obtained using our method. We think that the level of detail we achieve gives a comprehensive picture of the bifurcation structure of the problem, while keeping the analysis simple. Our approach retains the biophysical meaning of the parameters in the process of reduction, which allows for precise interpretation of various dynamical patterns.

To illustrate our approach we choose a three-variable model of an excitable cell introduced by Chay [6]. The model in [6] is a unified model for both the neuronal and secretory excitable membranes [8,39–41]. We shall refer to it as the Chay model. It captures many features of a more detailed physiological model of a pancreatic β-cell, the Chay–Keizer model [8]. In addition to providing a mathematical description for a complex and important physiological system (β-cells of the pancreas secrete insulin, a hormone that maintains the glucose blood level within narrow range), it captures several essential features common to many other models of bursting neurons. In this respect, we mention models of pyramidal cells in the neocortex [47,48], thalamic cells [32,37] and those of cells in the pre-Botzinger complex involved in the control of respiration [5]. These models possess similar dynamical mechanisms for bursting, although the ionic bases may be different. Another interesting feature of the Chay model is that it nicely illustrates the mechanism, by which calcium current controls the modes of activity in neural cells. We show that the variation of the maximal conductance of the voltage-dependent calcium current results in the transition from tonic spiking to bursting, as well as in the transitions between various bursting regimes (Fig. 1). Therefore, our results may be relevant to other models of neural cells involving calcium dynamics.

Bursting oscillations are ubiquitous in the experimental and modeling studies of excitable cells (see [5,8,10,13,14,32,37,39–41,47–49] and references therein). Biological significance and dynamical complexity of bursting oscillations stimulated mathematical investigations of the mechanisms of bursting behaviors [1,3,6,7,9,12–15,17,19,20,30,31,33–35,42,43,45,46,49,51]. Even minimal 3D models of bursting neurons exhibit a variety of periodic and aperiodic regimes under the variation of parameters. In particular, windows of chaotic dynamics were identified in the transitions from tonic spiking to bursting and in between different bursting regimes in a class of models of excitable membranes [1,6,7,9,34]. In [45,46], Terman rigorously showed the existence of chaotic regimes in a three-variable model of a bursting neuron. The analyses in [45,46] used 2D flow-defined maps near a homoclinic connection. Belykh et al. [3] proposed several mechanisms for the onset of bursting using 2D flow-defined maps. Recent studies of the transitions from bursting to continuous spiking in [42,43] showed that such transitions may involve highly nontrivial bifurcation scenarios such as the blue-sky catastrophe and the Lukyanov–Shilnikov bifurcations. Therefore, a comprehensive description of the dynamical phenomena associated with the transitions between different periodic regimes in the models of bursting neurons presents a challenging problem. Our study is motivated by numerical results showing that one-dimensional first return maps constructed for the slow variable account for various periodic and aperiodic regimes in a class of models. This approach was used in [1,6,7,34] to explain the origins of the chaotic dynamics in certain models. One-dimensional maps provide a valuable tool for studying oscillatory dynamics in a variety of biological and physical models (see, e.g., [22,25,26,28,38,44,52]). In the present paper, our goal was to derive the first return map for the dynamics of the slow variable in the Chay model and to study its properties analytically. Our approach is similar to that used by Rinzel and Troy in their studies of the bursting patterns in a model for the Belousov–Zhabotinsky reaction [35,36]. In [27], we used a similar approach to analyze the bifurcation structure of the family of mixed-mode periodic solutions for a compartmental model of the dopamine neuron. As in [27], the first return map for the Chay model is computed using two functions of cal-

cium concentration: the period of oscillations and the average value of the voltage-dependent calcium current when the concentration of calcium is kept constant. We were able to obtain detailed information about these functions using the results from the geometric theory for differential equations [21,23] and bifurcation theory [16,24]. For all practical purposes, these functions can be computed numerically. The latter approach may be useful in analyzing higher dimensional models, for which analytical methods may not be available. We also envision that in certain cases these functions can be evaluated directly from the experimental data. We believe that our approach will be useful for understanding mechanisms for firing patterns in a broad class of models.

The outline of the paper is as follows. In Section 2, we describe the Chay model and present numerical examples of the different spiking and bursting patterns generated by the model. Following [34], we identify the fast and the slow subsystems by separating timescales. Section 3 contains the bifurcation analysis of the two-dimensional fast subsystem. We show that under the variation of the control parameter, the fast subsystem undergoes a supercritical Andronov–Hopf (AH) bifurcation, followed by a saddle-node (SN) bifurcation and a homoclinic (HC) bifurcation. This information is used in Section 4, where we derive a one-dimensional first return map for the slow variable, the concentration of calcium. In Section 5, we analyze the bifurcations in a one-parameter family of the first return maps and relate them to the transitions between different spiking and bursting regimes. Finally, several natural generalizations of our results are given in Section 6.

2. The model

The model in [6] describes the dynamics of the membrane potential, $\tilde{v}(t)$, and calcium concentration, $u(t)$, in a cell with voltage-dependent sodium, potassium, and calcium channels, and calcium-dependent potassium channels:

$$\frac{\mathrm{d}\tilde{v}}{\mathrm{d}\tilde{t}} = g_I \tilde{m}_\infty^3(\tilde{v})\tilde{h}_\infty(\tilde{v})(\tilde{E}_I - \tilde{v}t) + g_{\mathrm{KV}} n^4(\tilde{E}_K - \tilde{v}) + \frac{g_{\mathrm{KC}} u}{1+u}(\tilde{E}_K - \tilde{v}) + g_L(\tilde{E}_l - \tilde{v}), \tag{2.1}$$

$$\frac{\mathrm{d}n}{\mathrm{d}\tilde{t}} = \frac{\tilde{n}_\infty(\tilde{v}) - n}{\tilde{\tau}(\tilde{v})}, \tag{2.2}$$

$$\frac{\mathrm{d}u}{\mathrm{d}\tilde{t}} = \tilde{\rho}(\tilde{m}_\infty^3(\tilde{v})\tilde{h}_\infty(\tilde{v})(\tilde{E}_{\mathrm{Ca}} - v) - \tilde{\gamma}u). \tag{2.3}$$

The first equation is the current balance equation, where the first term models effective conductance through the calcium and sodium channels. The activation of the voltage-dependent potassium channels changes according to (2.2). The calcium dynamics is modeled by the last equation. The intracellular calcium concentration, $u(t)$, is scaled by its dissociation constant and is a nondimensional variable. To have a better picture of the timescales associated with Eqs. (2.1)–(2.3), we rescale $\tilde{v}$ and $\tilde{t}$: $\tilde{v} = k_v v$ and $\tilde{t} = k_t t$, where $k_v = 10\,\mathrm{mV}$ and $k_t = 1/230\,\mathrm{s}^{-1}$. Using these changes of variables and by dividing both sides of (2.1) by g_{KV} we obtain the following system of equations:

$$\epsilon\dot{v} = a m_\infty^3(v)h_\infty(v)(E_I - v) + n^4(E_K - v) + \frac{\delta u}{1+u}(E_K - v) + l(E_l - v), \tag{2.4}$$

$$\dot{n} = \frac{n_\infty(v) - n}{\tau(v)}, \tag{2.5}$$

$$\dot{u} = \alpha(\gamma^{-1} m_\infty^3(v)h_\infty(v)(E_{\mathrm{Ca}} - v) - u), \tag{2.6}$$

where

$$\epsilon = (g_{\mathrm{KV}}k_t)^{-1}, \quad a = \frac{g_I}{g_{\mathrm{KV}}}, \qquad l = \frac{g_L}{g_{\mathrm{KV}}}, \qquad \alpha = \rho\gamma, \qquad \gamma = \frac{\tilde{\gamma}}{k_v}, \qquad \rho = \tilde{\rho}k_v k_t, \quad \text{and} \quad \delta = \frac{g_{\mathrm{KC}}}{g_{\mathrm{KV}}}.$$

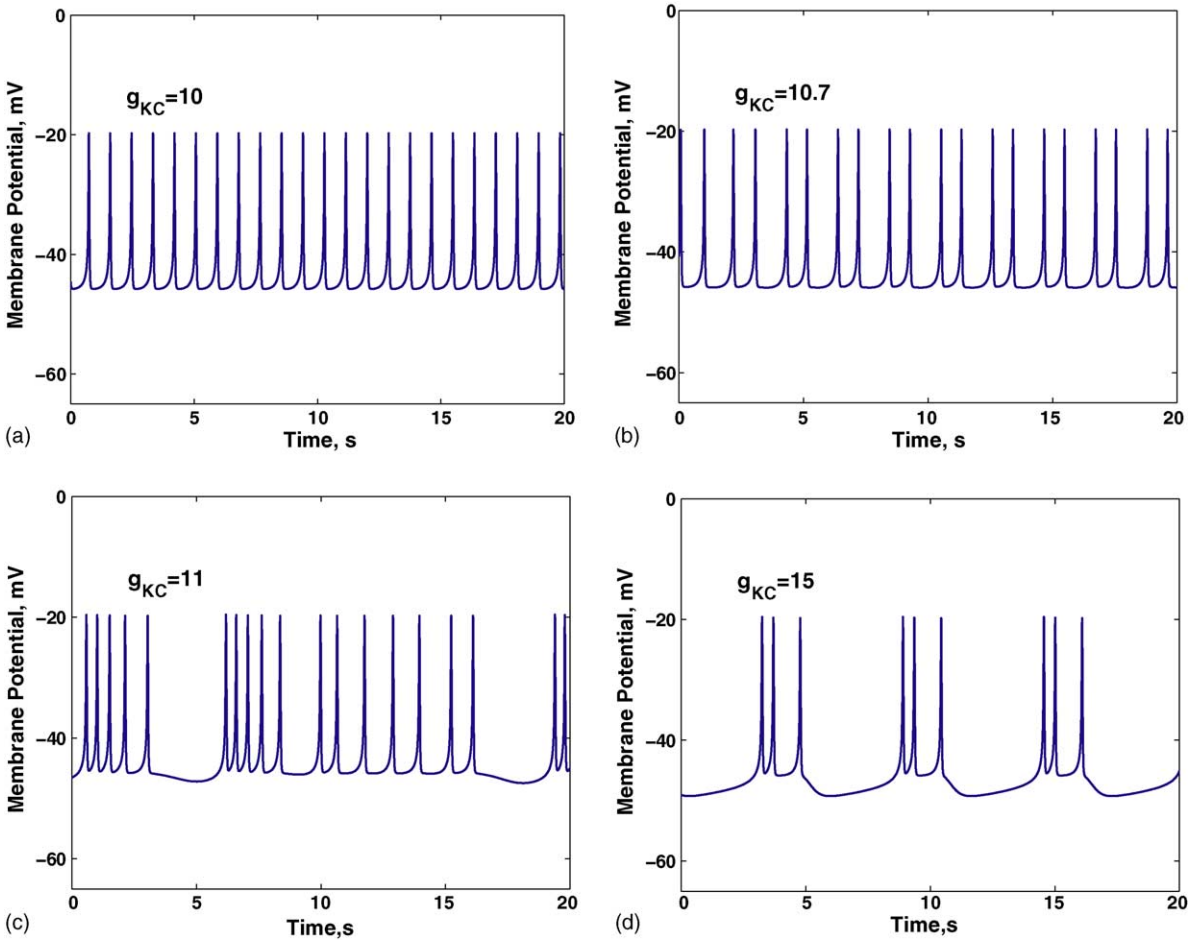

Fig. 1. Plots of the time series of $\tilde{v}(\tilde{t})$ for different values of g_{KC} demonstrate several firing patterns generated by (2.1)–(2.3): rhythmic single spiking, doublets, irregular and rhythmic bursting.

For the values of parameters of the original model (2.1)–(2.3) we refer to [6]. In Appendix A, we present the parameter values for the nondimensional model (2.4)–(2.6) and the analytical expressions for the functions m_∞, h_∞, n_∞, and τ. The latter have typical sigmoid forms similar to the corresponding functions in the Hodgkin–Huxley model. In [6], it was shown numerically that by varying g_{KC} in the range 10–30 s^{-1}, system of equations (2.1)–(2.3) has a variety of periodic and chaotic spiking and bursting solutions (Fig. 1). Following [6], we shall study the bifurcations of the periodic solutions of (2.4)–(2.6), using δ as a control parameter.

Remark 2.1. It is interesting to note that the coefficients in front of the first two terms on the right-hand side of (2.4) are close to 1, whereas the last two terms have coefficients $\sim 10^{-3}$ to 10^{-2}. Since the system of equations (2.4)–(2.6) is close to several bifurcations, the smaller terms are significant on the scale set by the distance of the system to the closest bifurcation in the parameter space. Therefore, they cannot be neglected.

System (2.4)–(2.6) is a singularly perturbed system of equations [21,29]. Our analysis uses the disparate timescales of the system dynamics, which are set by the small positive parameters α and ϵ. Specifically, we separate the equations in (2.4)–(2.6) into the *fast* and *slow subsystems*. The former is obtained by viewing u in (2.4) and

(2.5) as a parameter, i.e., by formally setting $\alpha = 0$:

$$\epsilon \dot{v} = am_\infty^3(v)h_\infty(v)(E_K - v) + n^4(E_K - v) + \frac{\delta u}{1+u}(E_K - v) + l(E_l - v), \tag{2.7}$$

$$\dot{n} = \frac{n_\infty(v) - n}{\tau(v)}. \tag{2.8}$$

The remaining equation (2.6) forms the slow subsystem. Below we show that in the range of parameters of interest the fast subsystems generates oscillations in v. Therefore, Eq. (2.6) is in the form suitable for application of the method of averaging [4,16]. In Section 4, we derive a map for the change in u after one cycle of oscillations of the fast subsystem:

$$\tilde{u} = P(u). \tag{2.9}$$

The study of the dynamics and bifurcations in the original system (2.1)–(2.3) is then reduced to the analysis of the one-dimensional map (2.9).

3. Analysis of the fast subsystem

In the present section, we use phase plane techniques to determine the bifurcations in (2.7) and (2.8) under the variation of

$$\beta = \frac{\delta u}{1+u}, \tag{3.1}$$

where u is fixed. It turns out that the system resides in the vicinity of the two bifurcations: a supercritical AH bifurcation and a HC bifurcation. Near these bifurcations the properties of the periodic orbits follow from the well-known results of the bifurcation theory [16,24]. We use this information in the next section to obtain the qualitative properties of the map in (2.9) and to determine the bifurcations of (2.9) under the variation of δ.

The fast subsystem is in turn a singularly perturbed system of two equations. For small $\epsilon > 0$, the dynamics of (2.7) and (2.8) can be deduced using the geometric methods for singularly perturbed systems [21,29]. For 2D systems, such as (2.7) and (2.8), a great deal of information can be obtained from the nullcline configuration in the phase plane. The v- (n-)nullcline in the phase plane of (2.7) and (2.8) is the set of points where $\dot{v}$ ($\dot{n}$) vanishes. By setting the right-hand sides of the Eqs. (2.7) and (2.8) to zero, we obtain the equations for the nullclines:

$$n^4 = \frac{am_\infty^3(v)h_\infty(v)(E_I - v) + l\,(E_l - v)}{v - E_K} - \beta \quad \text{and} \quad n = n_\infty(v), \tag{3.2}$$

where β is defined in (3.1).

In the range of parameters of interest equations in (3.2) define two curves in the n–v plane. Note that in n^4–v plane the variation of β results in a simple translation of the v-nullcline in vertical direction. Using this observation, we determine the following sequence of events:

(a) For negative values of β near 0, the nullclines intersect at a single point $(v_1(\beta), n_1(\beta))$, $n_1(\beta) = n_\infty(v_1(\beta))$. Since the point of intersection lies to the right of the point of maximum of the v-nullcline (i.e., on the stable branch of the slow manifold of (2.7) and (2.8)), it is a stable fixed point (Fig. 2a).
(b) As β increases, the v-nullcline moves down and $v_1(\beta)$ moves to the left. After it passes the point of the maximum of the v-nullcline, $v_{\max}$, there is a supercritical AH bifurcation at $\beta = \beta_{\mathrm{AH}}$ (Fig. 2b).
(c) As β increases further, the lower knee of the v-nullcline touches the n-nullcline at $\beta = \beta_{\mathrm{SN}}$. This corresponds to a saddle-node (SN) bifurcation. It creates two fixed points: $(v_2(\beta), n_2(\beta))$ and $(v_3(\beta), n_3(\beta))$, $n_{2,3} = n_\infty(v_{2,3}(\beta))$, $v_2(\beta) > v_3(\beta)$. The former is unstable and is moving to the right for increasing β (Fig. 2c).

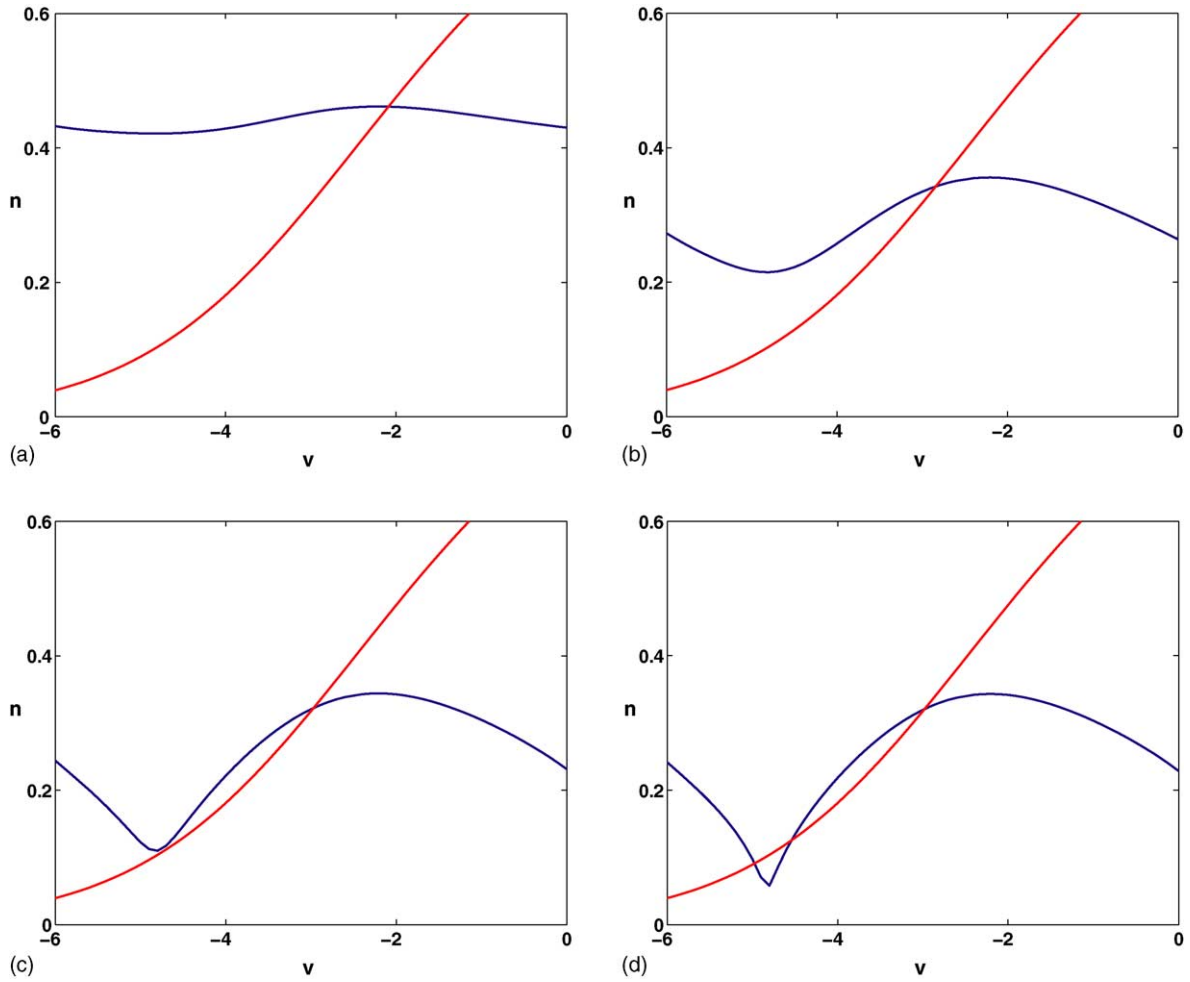

Fig. 2. The changes in the nullcline configuration for increasing values of β reflect the sequence of the bifurcations in the fast subsystem. A supercritical AH bifurcation takes place as the nullcline configuration in (a) changes to that in (b). Plots in (c) and (d) correspond to a SN and a HC bifurcations respectively.

(d) If β is increased further, at $\beta = \beta_{\mathrm{HC}}$, the unstable fixed point "collides" with the growing periodic orbit born at the AH bifurcation. This results in creation of a homoclinic orbit emanating from $(v_2(\beta_{\mathrm{HC}}), n_2(\beta_{\mathrm{HC}}))$. Thus, at $\beta = \beta_{\mathrm{HC}}$, $\beta_{\mathrm{HC}} > \beta_{\mathrm{SN}} > \beta_{\mathrm{AH}}$, there is a HC bifurcation (Fig. 2d).

(e) For $\beta > \beta_{\mathrm{HC}}$, the system becomes excitable with a single attracting fixed point $(v_3(\beta), n_3(\beta))$ and no periodic orbits. The v-coordinate of the stable fixed point, $v_3(\beta)$, moves to the left as β increases. The value of $v_3(\beta)$ is determined as the smallest root of the equation:

$$n^4(v) = \frac{a m_\infty^3(v) h_\infty(v)(E_I - v) + l(E_l - v)}{v - E_K} - \beta.$$

Therefore, in the range of parameters of interest, there are three bifurcations of the fixed points and periodic orbits in the fast subsystem: AH, SN, and HC bifurcations (Fig. 3)).

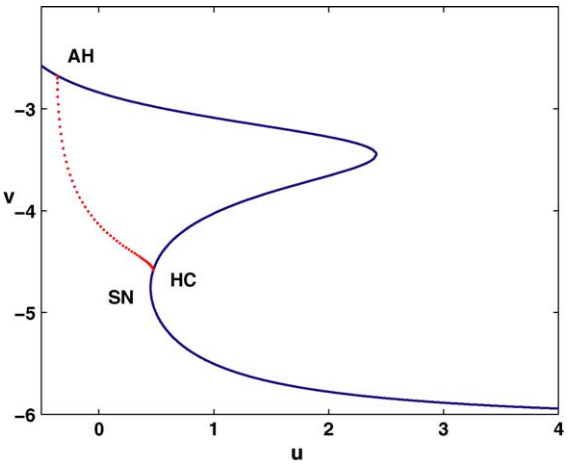

Fig. 3. The bifurcation diagram for the fast subsystem (2.7) and (2.8). The dotted line corresponds to the minimal values of $v(t)$ taken on the periodic orbits from the family of solutions born at the AH bifurcation and terminated at the HC bifurcation. The S-shaped curve corresponds to a curve of fixed points. For computational convenience, we used u as a bifurcation parameter to generate this diagram. Clearly, the diagram does not change qualitatively, if one uses β as a control parameter instead of u, because β is a monotone function of u.

Remark 3.1.

(a) The bifurcation diagram in Fig. 3 was obtained with numerical continuation software XPPAUT [11]. However, the qualitative form of this bifurcation diagram follows from the considerations presented in (a)–(e). Moreover, the values of β_{AH} and β_{SN} can be estimated analytically, using standard methods of the bifurcation theory [16,24]. We do not perform these calculations, because the qualitative information obtained with the phase plane analysis is sufficient for our purposes.

(b) The family of periodic orbits emanating from the AH bifurcation may undergo a saddle-node of limit cycles bifurcation before it limits onto the branch of equilibria. This situation is discussed in Section 6. In the main part of the paper, we assume that the limit cycles retain stability up to the HC bifurcation at $\beta = \beta_{\mathrm{HC}}$.

For construction of map (2.9), we need to review some properties of periodic orbits near a supercritical AH and HC bifurcations. In 2D singularly perturbed systems, such as (2.7) and (2.8), a periodic orbit born at a supercritical AH bifurcation undergoes a canard transition in a neighborhood of the AH bifurcation [23]. This transition is determined by the local vector field near the AH bifurcation point. For sufficiently small $\epsilon \to 0$, Theorem 3.3 in [23] implies the following properties of the canard cycles:

(C0) For $\beta > \beta_{\mathrm{AH}}$ and close to β_{AH}, there is a unique limit cycle $Z_\beta(\epsilon)$, which converges to a singular cycle Z_β in Hausdorff metric, as $\epsilon \to 0$. The shape of Z_β is determined by the v-nullcline (3.2) as shown in Fig. 4a.

(C1) In addition, if the conditions of Theorem 3.4 of [23] are satisfied, the canard cycles Z_β are asymptotically stable and their amplitudes grow monotonically with β. Here we refer to the condition involving the "way-in–way-out" function (Theorem 3.4 of [23]). This condition can be verified by a straightforward albeit tedious calculation. For all practical purposes, it can be easily checked numerically. Henceforth, we assume that this condition holds for (2.7) and (2.8).

Remark 3.2. Although for the value of $\epsilon \sim 0.1$, used in the Chay model, the periodic trajectories substantially deviate from those in the singular limit $\epsilon \to 0$, the qualitative features of the family of periodic orbits are captured by the family of singular trajectories. Alternatively, this family can be described by viewing the fast subsystem as a

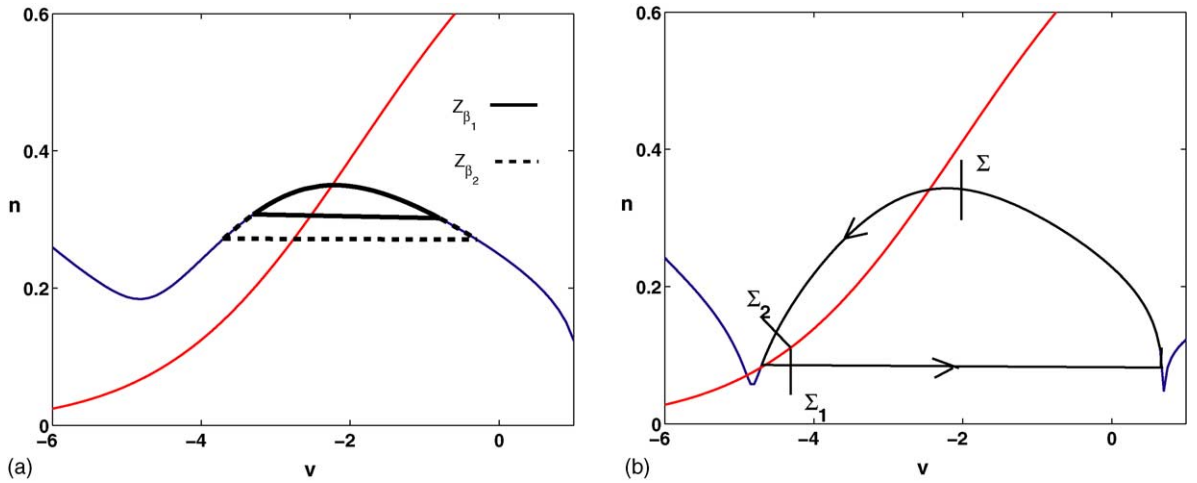

Fig. 4. (a) Canard cycles Z_{β_1} and Z_{β_2}, $\beta_2 > \beta_1$. (b) The local sections $\Sigma_{1,2}$ are transversal to the unstable and stable manifolds of the saddle $(v_2(\beta_{\mathrm{HC}}), n_2(\beta_{\mathrm{HC}}))$, respectively. The time of flight from Σ_1 to Σ_2 along the homoclinic orbit is T_0. Local sections $\Sigma_{1,2}$ split the periodic orbits of the fast subsystem near a HC bifurcation ($\beta < \beta_{\mathrm{HC}}$) into two parts: inside and outside some neighborhood of the saddle. The time of flight along the latter part is approximated by T_0.

perturbed Lienard equation, as was done in [31]. The latter approach yields better quantitative estimates. However, since the qualitative description of the family of periodic orbits using the singular limit $\epsilon \to 0$ is simpler and since we are only interested in the qualitative properties of this family of orbits, we use the former approach.

The statements in (C0) and (C1) give us necessary information about Z_β for β near β_{AH}. On the other hand, for β close to β_{HC} ($\beta < \beta_{\mathrm{HC}}$), the properties of Z_β follow from the well-known facts about the HC bifurcation in 2D systems [16,24,50]:

(HC) Let $s(\beta)$, $\beta \in (\beta_{\mathrm{SN}}, \beta_{\mathrm{HC}})$, denote a split function, which measures the distance between the branches of stable and unstable manifolds emanating from $(v_2(\beta), n_2(\beta))$ (see [24] for the definition of the split function). We assume that $s'(\beta_{\mathrm{HC}}) = -\mathrm{d} \neq 0$. In addition, Σ_1 and Σ_2 denote two local cross-sections, which are sufficiently close to saddle $(v_2(\beta_{\mathrm{HC}}), n_2(\beta_{\mathrm{HC}}))$ and are transversal to the unstable and stable manifolds, respectively (see Fig. 4b). Then for $\beta \to \beta_{\mathrm{HC}} - 0$, the period of the attracting limit cycle Z_β grows logarithmically:

$$\mathcal{T}(\beta) = T_0 - \mu \log s(\beta) + \text{higher order terms (h.o.t.)}, \tag{3.3}$$

where T_0 is the time of flight from Σ_1 to Σ_2 along the homoclinic orbit (see Fig. 4b), and $\mu^{-1} > 0$ is the positive eigenvalue of the matrix of linearization of (2.7) and (2.8) with $\beta = \beta_{\mathrm{HC}}$ about $(v_2(\beta_{\mathrm{HC}}), n_2(\beta_{\mathrm{HC}}))$. By plugging in

$$s(\beta) = \mathrm{d}(\beta_{\mathrm{HC}} - \beta) + \mathrm{o}(\beta_{\mathrm{HC}} - \beta)$$

into (3.3) we obtain

$$\mathcal{T}(\beta) = T_0 - \mu \log(\mathrm{d}(\beta_{\mathrm{HC}} - \beta)) + \mathrm{h.o.t.} \tag{3.4}$$

From (C1) and (HC), we conclude that the amplitude of Z_β and the period $\mathcal{T}(\beta)$ increase monotonically for $\beta \in (\beta_{\mathrm{AH}}, \beta_{\mathrm{HC}})$.

4. The first return map

Our goal in the present section is to derive a first return map for the dynamics of slow variable u, calcium concentration. We denote the first return map by

$$\tilde{u} = P(u) \tag{4.1}$$

and give a precise definition of P below. Map $P(u)$ reflects the changes of the calcium concentration after distinct events in the dynamics of the fast subsystem. Specifically, it shows how each spike within a burst affects the calcium concentration and how the latter changes after the period of quiescence. In the previous section, we identified the bifurcation structure of the fast subsystem and described the qualitative features of the family of periodic orbits, which supports spiking and bursting behaviors of the full 3D model (2.4)–(2.6). In particular, we showed that the period of oscillations $\mathcal{T}(\beta)$ is a monotone function tending to ∞, as $\beta \to \beta_{\mathrm{HC}} - 0$. These properties naturally translate into the qualitative form of the first return map. Our main observation about the structure of P is that its domain of definition can be split into three regions according to the qualitative form of P. These are the left-outer region, I^-, the inner region, I^0, and the right-outer region, I^+ (Fig. 5). The form of P in each of these regions reflects the properties of the attractors in the fast subsystem before, near, and past the HC bifurcation. A typical example of P is shown in Fig. 5. An examination of Fig. 5 shows that in the left-outer region, I^-, P is close to a linear map with the slope slightly less than 1. The iterations of P in I^- form an increasing sequence, which corresponds to a monotone increase in the calcium concentration during a burst. In the right-outer region, I^+, P is approximately constant (see also Remark 5.3b). The value of P in I^+ corresponds to the calcium concentration at the end of the quiescent phase. The structure of P in the boundary layer I^0 is determined by the properties of the periodic orbits of the fast subsystem near the HC bifurcation. We show that, in I^0, P is unimodal with the slope tending to $-\infty$ at the border between I^0 and I^+. This information about the qualitative form of P will be useful in Section 6, where we study the bifurcations of the fixed point and stable periodic orbits in a family of discrete 1D dynamical systems (4.1). In Section 6, we will also relate the results of the bifurcation analysis for (4.1) to spiking and bursting regimes of the original system of ordinary differential equations (2.4)–(2.6) and to transitions between them.

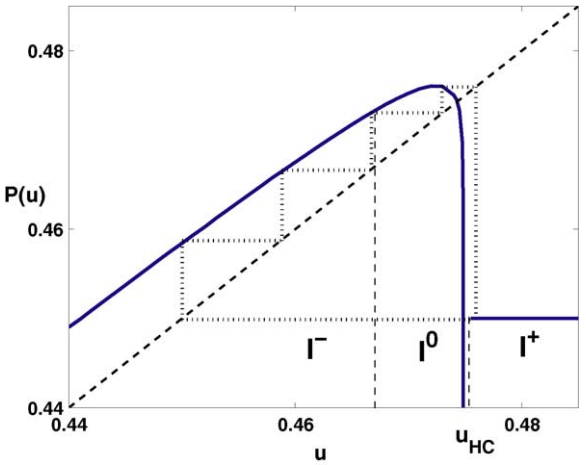

Fig. 5. Three regions in the domain of definition of P: the left-outer region, I^-, the inner region, I^0, and the right-outer region, I^+.

After these preliminary remarks we proceed with the derivation of the first return map. First, we make our definition of P precise. For this, we need the following auxiliary definitions:

$$u_y = \frac{\beta_y}{\delta - \beta_y}, \quad y \in \{\mathrm{AH}, \mathrm{HC}, \mathrm{SN}\}, \tag{4.2}$$

$$T(u) = \mathcal{T}(\beta), \quad \text{where } \beta = \frac{\delta u}{1+u}.$$

In the n–v plane we take a local section Σ, which is transversal to the v-nullcline, as shown in Fig. 4b. As before, by Z_β, $\beta_{\mathrm{AH}} < \beta < \beta_{\mathrm{HC}}$ we denote singular canard cycles lying inside the homoclinic orbit. Let $\xi \in (u_{\mathrm{AH}}, u_{\mathrm{HC}})$ and $(v_0, n_0) = \Sigma \cap Z_\beta$, with $\beta = \delta\xi(1+\xi)^{-1}$. Next we integrate (2.4)–(2.6) with initial condition (v_0, n_0, ξ). Map P is defined by

$$P(\xi) = u(T(\xi)),$$

where $T(\xi)$ is the time of the first return, i.e.,

$$T(\xi) = \min\{t > 0 : (v(t), n(t)) \in \Sigma \text{ and } \phi(t) \cdot e_2 < 0\}, \quad \phi(t) = (\dot{v}(t), \dot{n}(t)), \ e_2 = (0, 1),$$

and $\cdot$ denotes the scalar multiplication in $\mathbb{R}^2$.

From (2.6) we have

$$P(\xi) = \mathrm{e}^{-\alpha T(\xi)}\xi + \rho \int_0^{T(\xi)} f(v(s))\, \mathrm{e}^{\alpha(s-T(\xi))}\, \mathrm{d}s, \tag{4.3}$$

where $\rho = \alpha\gamma^{-1}$ and

$$f(v) = m_\infty^3(v) h_\infty(v)(E_{\mathrm{Ca}} - v).$$

We rewrite (4.3) as

$$P(\xi) = \mathrm{e}^{-\alpha T(\xi)}\xi + \rho \bar{f}(\xi) \int_0^{T(\xi)} \mathrm{e}^{\alpha(s-T(\xi))}\, \mathrm{d}s = \mathrm{e}^{-\alpha T(\xi)}\xi + (1 - \mathrm{e}^{-\alpha T(\xi)})F(\xi), \tag{4.4}$$

where

$$\bar{f}(\xi) = \frac{\int_0^{T(\xi)} f(v(s))\, \mathrm{e}^{\alpha(s-T(\xi))}\, \mathrm{d}s}{\int_0^{T(\xi)} \mathrm{e}^{\alpha(s-T(\xi))}\, \mathrm{d}s} \quad \text{and} \quad F(\xi) = \frac{\bar{f}(\xi)}{\gamma}.$$

The structure of map (4.4) is determined by two functions of calcium concentration: the period of oscillations, $T(\xi)$, and the weighted average amount of calcium entering the cell with the voltage-dependent calcium current during one cycle of oscillations scaled by the calcium removal constant, $F(\xi)$. Note that $F(\xi)$ must be O(1) in the context of this model, because it represents the ratio of the rate of the voltage-dependent calcium current and that of its removal. If one of these quantities is significantly bigger than the other, the calcium dynamics will be trivial. Near the HC bifurcation, the period of oscillations of the fast system changes drastically. This creates three regions in the domain of definition of P, over which it has qualitatively different form. To introduce these regions, we

define

$$u_0 = \frac{\beta_0}{\delta - \beta_0}, \quad \text{where } \beta_0 : \mathcal{T}(\beta_0) = T_0,$$

where T_0 is defined in (3.3).

We distinguish the following regions in the domain of definition of P:

(a) *The left-outer region*: $I^- = [0, u_0]$.

By continuous dependence of solutions of (2.4)–(2.6) on α, for $\xi \in I^-$, we have

$$T(\xi) = T_0(\xi) + \mathrm{O}(\alpha), \tag{4.5}$$

$$(v(t), n(t)) = (v_0(t), n_0(t)) + \mathrm{O}(\alpha), \quad 0 \le t \le T(\xi), \tag{4.6}$$

where $(v_0(t), n_0(t))$, $t > 0$ is the periodic solution of the fast subsystem with initial condition (v_0, n_0) and $u = \xi$ and $T_0(\xi)$ is its period. By plugging in (4.5) and (4.6) into (4.4) and using the Taylor's expansion for the exponential function, we obtain

$$P(\xi) = (1 - \alpha T_0(\xi))\xi + \alpha T_0(\xi) F(\xi) + \mathrm{O}(\alpha^2), \quad \xi \in I^-. \tag{4.7}$$

Therefore, in the left-outer region, for sufficiently small α, $P(\xi)$ is close to a linear map with a positive slope less than 1 (see Fig. 5).

(b) *The inner region*: $I^0 = [u_0, u_{\mathrm{HC}}]$.

In the inner region, the period of oscillations of the fast subsystem (2.7) and (2.8), $T_0(\xi)$ grows without bound. To obtain a uniform approximation of the trajectory of $(v(t), n(t), u(t))$ for $\xi \in I^0$. We modify the construction of the first return map. In the n–v plane we use two sections Σ_1 and Σ_2 that divide the periodic orbits of the fast subsystem near the HC bifurcation into two parts (see Fig. 4b):

(1) The portion lying outside a neighborhood of the homoclinic point $(v_{\mathrm{HC}}, n_{\mathrm{HC}})$, where $v_{\mathrm{HC}} = v_2(\beta_{\mathrm{HC}})$, $n_{\mathrm{HC}} = n_\infty(v_{\mathrm{HC}})$. The time of flight of the phase point of the fast subsystem along this portion of the periodic orbit to leading order does not depend on u and is approximately equal to T_0, the time of flight along the corresponding portion of the homoclinic orbit for $u = u_{\mathrm{HC}}$.

(2) The remaining part of the periodic orbit lies in a small neighborhood of $(v_{\mathrm{HC}}, n_{\mathrm{HC}})$.

As before, we define $P_1 : \mathbb{R} \to \mathbb{R}$ by taking the initial condition (v_0, n_0, ξ) such that $(v_0, n_0) \in Z_\beta \cap \Sigma_1$, $\beta = \delta\xi(1 + \xi)^{-1}$ and integrating (2.4)–(2.6) until the projection of the trajectory to the v–n plane hits Σ_2 at time $t = T_1(\xi)$. We define $P_1(\xi) = u(T_1(\xi))$. Similarly, we define P_2 by taking the initial condition whose projection onto v–n lies in Σ_2 and integrating (2.4)–(2.6) until the projection of the phase trajectory hits Σ_1. Finally, we define $P = P_2 \circ P_1$.

P_1 is computed as in (4.7):

$$P_1(\xi) = (1 - \alpha T_0)\xi + \alpha T_0 F_0 + \mathrm{O}(\alpha^2), \quad F_0 = \frac{1}{\gamma T_0} \int_0^{T_0} f(v(s))\, \mathrm{e}^{\alpha(s - T_0)}\, \mathrm{d}s. \tag{4.8}$$

Let $\xi_1 = P_1(\xi)$. To compute P_2, we rewrite (3.4):

$$T(\xi_1) - T_0 = -\mu \log\left(\mathrm{d}\left(\beta_{\mathrm{HC}} - \frac{\delta\xi_1}{1 + \xi_1}\right)\right) + \text{h.o.t.} \tag{4.9}$$

From (4.3) we have

$$P_2(\xi_1) = \mathrm{e}^{-\alpha(T(\xi_1) - T_0)}\xi_1 + \rho \int_{T_0}^{T(\xi_1)} f(v(s))\, \mathrm{e}^{\alpha(s - T(\xi_1))}\, \mathrm{d}s. \tag{4.10}$$

Note that, by (4.9),

$$\mathrm{e}^{-\alpha(T(\xi_1)-T_0)} = C(\alpha)\left(\beta_{\mathrm{HC}} - \frac{\delta\xi_1}{1+\xi_1}\right)^{\alpha\mu}, \quad \text{where } C(\alpha) = d^{\alpha\mu}(1+\mathrm{o}(1)) \to 1 \text{ as } \alpha \to 0. \tag{4.11}$$

$$\begin{aligned}\int_{T_0}^{T(\xi_1)} f(v(s))\,\mathrm{e}^{\alpha(s-T(\xi_1))}\,\mathrm{d}s &\approx f(v_{\mathrm{HC}})\int_{T_0}^{T(\xi_1)} \mathrm{e}^{\alpha(s-T(\xi_1))}\,\mathrm{d}s \\ &= \alpha^{-1} f(v_{\mathrm{HC}})\left(1 - C(\alpha)\left(\beta_{\mathrm{HC}} - \frac{\delta\xi_1}{1+\xi_1}\right)^{\alpha\mu}\right).\end{aligned} \tag{4.12}$$

By combining (4.10)–(4.12), we obtain

$$P_2(\xi_1) = C(\alpha)\left(\beta_{\mathrm{HC}} - \frac{\delta\xi_1}{1+\xi_1}\right)^{\alpha\mu}(\xi_1 - F_1) + F_1 + \text{h.o.t.}, \quad \text{where } F_1 = f(v_{\mathrm{HC}})\gamma^{-1}. \tag{4.13}$$

Note that, by (4.10) and (4.13),

$$P_2(\xi) = \begin{cases} \xi & \text{as } \xi \to u_0 + 0, \\ F_1 & \text{as } \xi \to u_{\mathrm{HC}} - 0. \end{cases}$$

Therefore, we have continuously extended P from the left-outer region through the inner region.

(c) Finally, we define *the right-outer region* for $\xi > u_{\mathrm{HC}}$. For this, we recall that for $u > u_{\mathrm{HC}}$, all trajectories of the fast subsystem (except that starting from the unstable fixed points) converge to a unique attracting equilibrium $(v_3(\beta), n_3(\beta))$, $\beta = \delta u(1+u)^{-1}$ (see Statement (e), Section 3). This observation combined with (2.6) yields

$$\dot{u} = \alpha(\gamma^{-1} f(\psi(u)) - u), \tag{4.14}$$

where $\psi(u) = v_3(\beta)$, $\beta = \delta u(1+u)^{-1}$. Using an argument commonly applied in the analysis of bursting [34], one shows that $(v_3(u), n_3(u))$ moves close to the stable branch of the fixed points parameterized by u, as u is slowly decreasing according to (4.14) until it reaches $u = u_{\mathrm{SN}}$. Therefore, we extend the definition of $P(\xi)$ for $\xi > u_{\mathrm{HC}}$ by

$$P(\xi) = u_{\mathrm{SN}} < u_{\mathrm{HC}}. \tag{4.15}$$

The last inequality follows from statements (c) and (d) of the previous section.

This completes the description of the first return map P.

5. Bifurcations of the first return map

In the present section, we study the bifurcations of the stable solutions of (2.4)–(2.6) under the variation of δ (or, in terms of the original system (2.1)–(2.3), for varying g_{KC}). The analysis of the previous section reduces this problem to the study of bifurcations in a one-parameter family of maps (4.1). A heuristic examination of P suggests that there are two main types of attractors of (4.1): a stable fixed point and a superstable cycle (see Fig. 5). Clearly, these two types of attractors of the discrete system correspond to spiking and bursting patterns generated by the original system (2.4)–(2.6). Our approach in this section is to locate a unique fixed point of P and to track its position under the variation of δ. In particular, we show that for small values of δ, the fixed point lies in the left-outer region, where it is necessarily stable, because the slope of the graph of $P(u)$ in I^- is less than 1. If δ is increased, the fixed point moves into the inner region. By following the fixed point as it moves through the inner region, we detect

the main events in the sequence of bifurcations of the discrete system. The first bifurcation in this sequence is a period-doubling (PD) bifurcation of the fixed point, which gives rise to a two-spike periodic solution (a doublet) of the continuous system (2.4)–(2.6) (see Fig. 1b). For larger values of δ, there exists a family of superstable cycles of P, which correspond to bursting solutions of the original system. For a piecewise-linear approximation of P, we show that the family of superstable cycles undergoes reverse period-adding bifurcations for increasing values of δ. This implies the order, in which different bursting solutions appear in the continuous system under the variation of control parameter. Finally, we comment on the possibility of complex dynamics in narrow windows in the parameter space lying between regions of existence of distinct bursting solutions. Therefore, the results of this section provide a comprehensive description of stable periodic solutions of the original system (2.4)–(2.6) and suggest mechanisms for transitions between them.

First, we show that there exists a unique fixed point of P in the range of parameters of interest and clarify its dependence on the control parameter δ. From (4.4), we obtain the equation for the fixed points of P:

$$F(u) = u. \tag{5.1}$$

It is convenient to rewrite this equation in terms of β:

$$\mathcal{F}(\beta) = \frac{\beta}{\delta - \beta}, \quad \text{where } \mathcal{F}(\beta) \equiv F\left(\frac{\beta}{\delta - \beta}\right). \tag{5.2}$$

As shown in Appendix B, function $\mathcal{F}(\beta)$ has the following properties:

(a) $\mathcal{F}(\beta)$ is a decreasing continuous function on $[0, \beta_{\mathrm{HC}}]$ with $\mathcal{F}(\beta_{\mathrm{HC}} - 0) = F_1$,
(b) $\mathcal{F}'(\beta_{\mathrm{HC}} - 0) = -\infty$.

In the remainder of this section, we will need the following definitions:

$$\beta_0: \quad \mathcal{T}(\beta_0) = T_0, \qquad \delta_0: \quad \frac{\beta_0}{\delta_0 - \beta_0} = \mathcal{F}(\beta_0), \quad \text{i.e., } \delta_0 = \beta_0(1 + \mathcal{F}(\beta_0)^{-1}), \tag{5.3}$$

$$\bar{\delta}: \quad \frac{\beta_{\mathrm{HC}}}{\delta - \beta_{\mathrm{HC}}} = \mathcal{F}(\beta_{\mathrm{HC}}), \quad \text{i.e., } \bar{\delta} = \beta_{\mathrm{HC}}(1 + \mathcal{F}(\beta_{\mathrm{HC}})^{-1}) \tag{5.4}$$

(see Fig. 6).

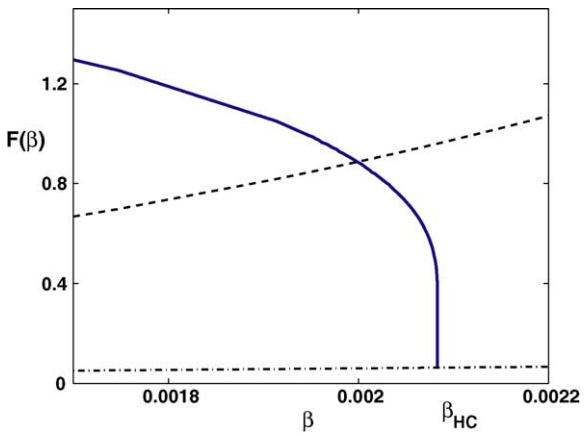

Fig. 6. The graphs of $\mathcal{F}(\beta)$ (solid line) and functions on the left-hand sides of (5.3) and (5.4) (dashed and dash-dotted lines, respectively).

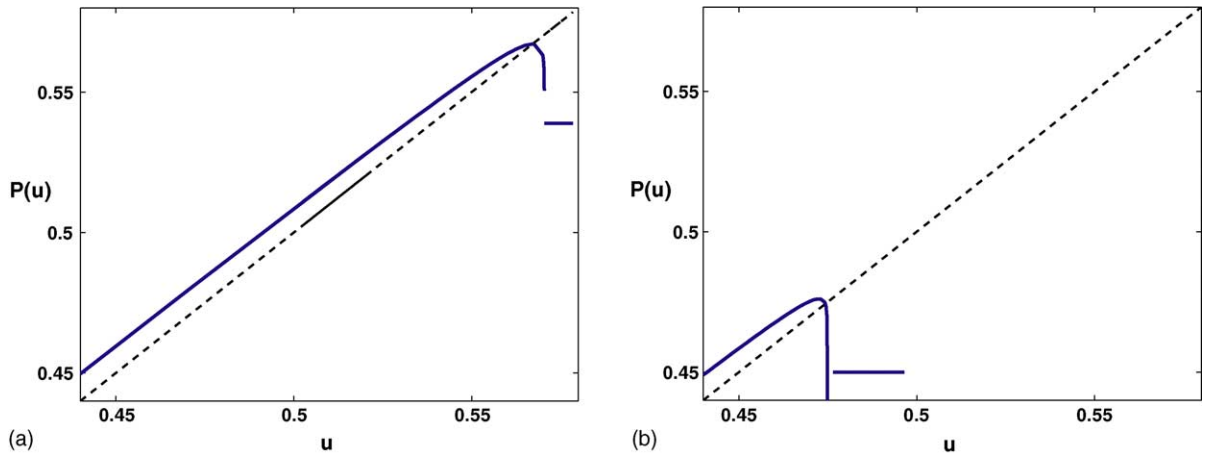

Fig. 7. The plots of P for two values of $\delta : \delta_1 < \delta_2$. Plots in (a) and (b) show the fixed point of P before and after the PD bifurcation.

5.1. The fixed point of P: regular spiking

Using monotonicity of functions on the both sides of (5.2), we conclude that (5.2) has a unique solution on $[0, \beta_{\mathrm{HC}}]$ provided

$$\mathcal{F}(\beta_{\mathrm{HC}}) \le \frac{\beta_{\mathrm{HC}}}{\delta - \beta_{\mathrm{HC}}} \quad (\text{or } F(u_{\mathrm{HC}}) \le u_{\mathrm{HC}}). \tag{5.5}$$

This implies that there is a unique solution $\bar{\beta}(\delta)$ of (5.2) for $0 \le \delta \le \bar{\delta}$. $\bar{\beta}(\delta)$ is a continuous increasing function on $[0, \bar{\delta}]$ and $\bar{\beta}(\delta) \to \beta_{\mathrm{HC}}$ as $\delta \to \bar{\delta} - 0$. Therefore, for $\delta \in [0, \bar{\delta}]$, P has a unique fixed point $\bar{u}(\delta) \in [0, u_{\mathrm{HC}}]$. Moreover, for $\delta \in [0, \delta_0]$ the fixed point lies in the left-outer region. It is easy to see that $\bar{u}(\delta)$ is attracting in this case.

Remark 5.1. Inequality (5.5) gives a sufficient condition for the oscillatory activity (both spiking and bursting) in (2.4)–(2.6). It has a simple biophysical interpretation: (5.5) requires that the voltage-dependent calcium current is dominated by the removal of calcium when calcium concentration is kept constant at $u = u_{\mathrm{HC}}$.

5.2. The period-doubling bifurcation: firing in doublets

As δ is increased from δ_0 to $\bar{\delta}$, the fixed point moves through the inner region. Below we show that it looses stability through a PD bifurcation at a certain value of control parameter $\delta = \delta_{\mathrm{PD}} \in (\delta_0, \bar{\delta})$ (Fig. 7). In terms of periodic solutions of continuous system (2.4)–(2.6), the PD bifurcation corresponds to the birth of a doublet, a two-spike periodic solution (see Fig. 1b).

By differentiating (4.4), we have

$$P'(u) = \alpha T'(u)\, \mathrm{e}^{-\alpha T(u)}(F(u) - u) + \mathrm{e}^{-\alpha T(u)} + F'(u)(1 - \mathrm{e}^{-\alpha T(u)}).$$

To locate the PD bifurcation of $\bar{u}(\delta)$, we set the derivative of P at $\bar{u}(\delta)$ to -1:

$$P'(\bar{u}(\delta)) = \mathrm{e}^{-\alpha T(\bar{u}(\delta))} + F'(\bar{u}(\delta))(1 - \mathrm{e}^{-\alpha T(\bar{u}(\delta))}) = -1. \tag{5.6}$$

In the equation above, we used (5.1) to simplify the expression for $P'(\bar{u})$. Next, we show that (5.6) has a solution in $(\delta_0, \bar{\delta})$. For this, we note that for δ varying from δ_0 to $\bar{\delta}$, the fixed point $\bar{u}(\delta)$ moves from u_0 to u_{HC}.

In addition,

$$P'(\bar{u}(\delta_0)) = P'(u_0) = \mathrm{e}^{-\alpha T_0} + F'(u_0)(1-\mathrm{e}^{-\alpha T_0}) = 1 - \alpha T_0 + \alpha F'(u_0)T_0 + \mathrm{O}(\alpha^2) = 1 + \mathrm{O}(\alpha) > -1. \tag{5.7}$$

On the other hand, as $\delta \to \bar{\delta} - 0$, $\bar{u}(\delta) \to u_{\mathrm{HC}} - 0$. By taking $\delta \to \bar{\delta} - 0$ in the expression of $P'(\bar{u}(\delta))$ in (5.6), we obtain

$$P'(\bar{u}(\bar{\delta} - 0)) = P'(u_{\mathrm{HC}} - 0) = -\infty < -1, \tag{5.8}$$

because $\lim_{u\to u_{\mathrm{HC}}-0} \mathrm{e}^{-\alpha T(u)} = 0$ and $\lim_{u\to u_{\mathrm{HC}}-0} F'(u) = -\infty$. By combining (5.6)–(5.8), we conclude that (5.6) has a solution on $(\delta_0, \bar{\delta})$. We denote the smallest solution of (5.6) on $(\delta_0, \bar{\delta})$ by δ_{PD}. Therefore, $\bar{u}(\delta)$ is attracting for $\delta \in (0, \delta_{\mathrm{PD}})$, $\delta_{\mathrm{PD}} < \bar{\delta}$, and it undergoes a PD bifurcation at $\delta = \delta_{\mathrm{PD}}$. The attracting period 2 cycle born at the PD bifurcation corresponds to a doublet solution of the original model (2.4)–(2.6) (Fig. 1b).

5.3. *Superstable cycles of P: bursting*

In the present section, we show that for sufficiently large $\delta \in (\delta_0, \bar{\delta})$, the first return map P has a family of superstable cycles, which correspond to bursting periodic solutions of continuous system (2.4)–(2.6). By studying the bifurcations of the cycles of discrete system we establish the order, in which the bursting patterns appear in continuous system (2.4)–(2.6) for increasing values of control parameter.

Bursting is generated by the first return maps whose iterations revisit the right-outer region, I^+. By regular (periodic) bursting we refer to superstable cycles of P of the form:

$$S_q = \{x_i, i = 1, 2, \ldots, q+1 : x_1 = P(u_{\mathrm{SN}}), x_q > u_{\mathrm{SN}}, x_{j+1} = P(x_j),\ j = 1, 2, \ldots, q-1\}.$$

A necessary and sufficient condition for regular bursting is given by

$$\exists k \in \mathbb{Z}^+ : P^k(u_{\mathrm{SN}}) \in J_1,$$

where $J_1 = \{u : P(u) > u_{\mathrm{HC}}\}$. We shall use the following observation:

(B) There exists $\delta_b \in (0, \bar{\delta})$ such that $\max_{u\in[0,u_{\mathrm{HC}}]} P(u) > u_{\mathrm{HC}}$ for $\delta \in (\delta_b, \bar{\delta})$.

Indeed, as we showed in Section 5.1, the fixed point of P, $\bar{u}(\delta) \to u_{\mathrm{HC}}$ as $\delta \to \bar{\delta} - 0$. On the other hand, by (5.8), $P'(\bar{u}) \to -\infty$ as $\delta \to \bar{\delta} - 0$. Therefore, statement in (B) holds.

From (B) we conclude that $J_1 \neq \emptyset$ for $\delta \in (\delta_b, \bar{\delta})$. We decompose the inner region, I^0, into three closed intervals:

$$I^0 = \bar{J}_0 \cup \bar{J}_1 \cup \bar{J}_2, \quad i \neq j, \qquad J_i \cap J_j = \emptyset, \quad i, j \in \{0, 1, 2\},$$

where open interval $J_0(J_2)$ lies to the left (right) of J_1. Note that the remarks following (B) imply that the size of J_2 tends to zero as $\delta \to \bar{\delta} - 0$ (compare Fig. 8a and b). Henceforth, we shall assume that $\delta \in (\delta_b, \bar{\delta})$ is sufficiently close to $\bar{\delta}$ so that the size of J_2 is sufficiently small. Our numerical results suggest that these assumptions hold for the most part of the interval in δ (g_{KC}) corresponding to bursting behavior in the Chay model (see Fig. 8b). Furthermore, the numerics gives a clear evidence that on $I^0 \cup \bar{J}_0$, P can be approximated well by a linear function. For such approximation, we choose

$$P_l(u) = Au + \alpha F_0 T_0, \quad \text{where } A = 1 - \alpha T_0. \tag{5.9}$$

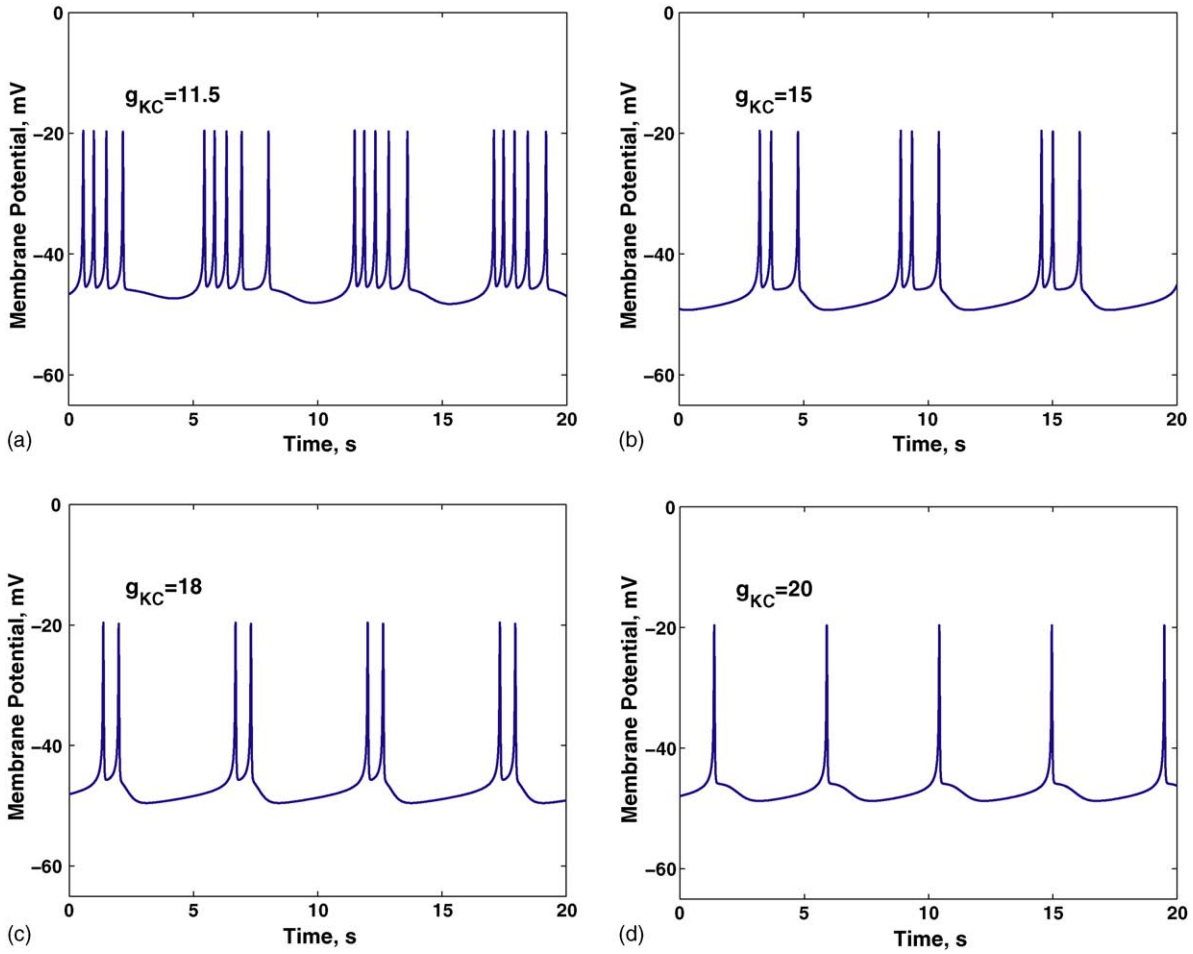

Fig. 8. The bursting patterns exhibit reverse period-adding for increasing values of g_{KC}.

Remark 5.2. Note that we only need that P_l be close to P on $I^- \cup \bar{J}_0$, because on J_1 the definition of P_l is irrelevant, as long as $P_l(u) > u_{\mathrm{HC}}$, and J_2 is very small. It can be shown that on I^-, P and P_l are $\mathrm{O}(\alpha)$ close in C^1-metric (see (4.7)). This statement can be extended to J_0 provided that J_0 lies sufficiently far away for u_{HC}.

We extend the definition of P_l to the rest of the inner region:

$$P_l(u) = \begin{cases} Au + \alpha F_0 T_0, & I^- \cup I^0, \\ u_{\mathrm{SN}}, & I^+. \end{cases} \tag{5.10}$$

With the assumptions that we made earlier, we reduce the study of the superstable cycles of P to those of P_l. For sufficiently small $\alpha > 0$, the implicit function theorem implies the existence of a superstable cycle S_q of P whenever P_l has a superstable cycle $\tilde{S}_q$ bounded away from J_2.

To study the superstable cycles of P_l we note that

$$P^k(u_{\mathrm{SN}}) = A^k u_{\mathrm{SN}} + \alpha T_0 F_0 (A^{k-1} + A^{k-2} + \cdots + 1) = (1 - k\alpha T_0) u_{\mathrm{SN}} + k\alpha T_0 F_0 + \mathrm{O}(\alpha^2). \tag{5.11}$$

Therefore, the region of existence of a superstable cycle $\tilde{S}_k$ of P_l is given by $\delta_k \le \delta < \delta_{k-1}$, where

$$\delta_k : \quad P_l^k(u_{\rm SN}) = u_{\rm HC} \quad \text{for } \delta = \delta_k. \tag{5.12}$$

Using (4.2) and (5.11), we rewrite (5.12) as follows:

$$(1 - k\alpha T_0)\frac{\beta_{\rm SN}}{\delta_k - \beta_{\rm SN}} + k\alpha T_0 F_0 = \frac{\beta_{\rm HC}}{\delta_k - \beta_{\rm HC}} + \text{h.o.t.} \tag{5.13}$$

From (5.13) we obtain

$$\delta_k = \beta_{\rm SN}(1 + F_0) + \frac{\beta_{\rm HC} - \beta_{\rm SN}}{\alpha k T_0} \cdot \frac{\delta_k}{\delta_k - \beta_{\rm HC}} + \text{h.o.t.} \tag{5.14}$$

By taking into account that $\delta \in (0.01, 0.02)$ and $\beta_{\rm HC} \approx 2.03 \times 10^{-3}$, we approximate

$$\frac{\delta_k}{\delta_k - \beta_{\rm HC}} \approx 1$$

and obtain

$$\delta_k \approx \beta_{\rm SN}(1 + F_0) + \frac{\beta_{\rm HC} - \beta_{\rm SN}}{\alpha k T_0}. \tag{5.15}$$

The last expression implies that the family superstable cycles of the piecewise-linear map P_l undergoes reverse period-adding bifurcations as $\delta \in (\delta_b, \bar{\delta})$ increases. From this we conclude that the superstable of P will undergo reverse period-adding bifurcations as well. Therefore, the number of spikes within one burst in the stable periodic bursting solutions appearing for increasing values of δ will decrease by 1 (see Fig. 8). Moreover, it is clear from the geometry of P, that prior to disappearance of a superstable cycle, one of its points approaches J_2, where the slope of P is negative and large in absolute value (see Fig. 9b and c). This implies that such superstable cycle will undergo a period-doubling bifurcation. As δ is increased further and while the branch of P with a steep negative slope is involved in the dynamics, one expects complex and possibly chaotic dynamics. However, the size of the windows of the control parameter, in which the complex dynamics takes place is of the same order as the size of J_2, i.e., is very small.

Remark 5.3.

(a) Note that the positive eigenvalue of the matrix of linearization of (2.7) and (2.8) about $(v_{\rm HC}, n_{\rm HC})$) with $\delta u/(1 + u) = \beta_{\rm HC}$, $\mu^{-1} \sim \epsilon^{-1}$. By taking $\epsilon \to 0$ in (4.13), we find that P_2 approaches a linear function on $I^0/\{u_{\rm HC}\}$. Therefore, the boundary layer shrinks to a point as $\epsilon \to 0$, and the piecewise-linear approximation of P is more accurate for smaller $\epsilon > 0$.

(b) In Section 3, we argued that in the right-outer region (ROR) P can be approximated by a constant function: $P(u) = u_{\rm SN}$. This statement holds in a singular limit $\epsilon \to 0$. For small positive values of ϵ, the graph of P over ROR will have a small negative slope. While this deviation of P from a constant map in the ROR has a small (perturbative) effect on the regions of existence of superstable cycles of P corresponding to periodic bursting, it becomes important for analyzing irregular bursting. Indeed, if P is constant in ROR then once the phase point has visited the ROR twice it belongs to a superstable periodic cycle corresponding to periodic bursting. This rules out chaotic bursting. However, if in ROR P deviates from constant function by an arbitrarily small amount, chaotic bursting is possible.

In conclusion, we mention that the bifurcation scenario described in the present section is consistent with the numerical and analytical results showing that chaotic regimes are present in the Chay model between windows of continuous spiking and bursting and between distinct periodic bursting regimes [1,6,7,9,45,46].

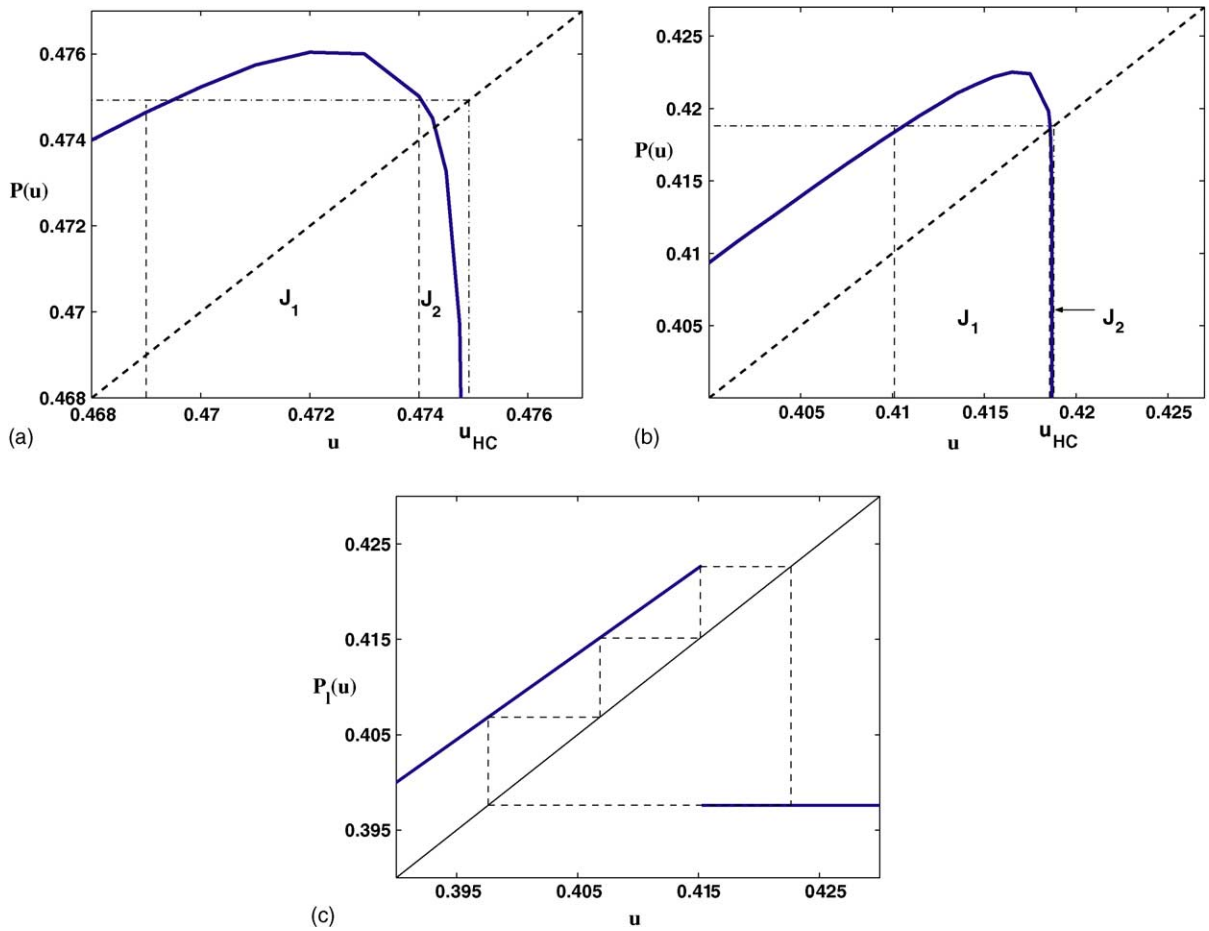

Fig. 9. The first return map corresponding to bursting patterns for $g_{KC} = 11$ (a) and $g_{KC} = 12$ (b). A piecewise-linear approximation of P is shown in (c)).

6. Discussion

The method of the present paper can be extended to analyze other models of bursting cells. In the this section, we discuss several generic situations closely related to the Chay model. There are four codimension-one bifurcations leading to the disappearance of a stable limit cycle [15,16]:

(HC) a homoclinic bifurcation,
(SNIC) a saddle-node on an invariant circle bifurcation,
(SNLC) a saddle-node of limit cycles bifurcation,
(AH) an Andronov–Hopf bifurcation.

Therefore, there are four (groups of) scenarios for the transition from the fast oscillations to the slow motion in the dynamics of the fast–slow bursting [15,20]. Here we assume that the transition from the slow motion along the branch of equilibria to the fast oscillations is realized through a SN bifurcation. In the first two scenarios, the period of oscillations grows without bound, and it remains finite in the last two ones. The first case of a HC bifurcation

was treated in the previous sections. Here we discuss the remaining cases. Our goal is to indicate the common features and to highlight the differences from the analyses in the previous sections, rather than to give an exhaustive description.

6.1. Saddle-node on an invariant circle

Suppose that the stable oscillations in the fast subsystem terminate through a SNIC bifurcation at $\beta = \beta_{\mathrm{SNIC}}$. The normal form for a SNIC bifurcation [24] implies that near the bifurcation the leading term in the asymptotic expansion for the period of oscillations is given by

$$\mathcal{T}(\beta) \approx T_0 + \frac{C}{\sqrt{\beta - \beta_{\mathrm{SNIC}}}}, \tag{6.1}$$

where

$$C = \frac{\pi}{\sqrt{ad}}, \quad a = \left.\frac{\partial^2 N(v, n_\infty(v), \beta_{\mathrm{SNIC}})}{\partial v^2}\right|_{v=v_{\mathrm{SNIC}}}, \quad d = \left.\frac{\partial N(v_{\mathrm{SNIC}}, n_\infty(v_{\mathrm{SNIC}}), \beta)}{\partial \beta}\right|_{\beta=\beta_{\mathrm{SNIC}}},$$

and $N(v, n_\infty(v), \beta)$ denotes the right-hand side of the equation for the membrane potential (2.7) and (3.1). As $\beta \to \beta_{\mathrm{SNIC}} - 0$, the period of oscillations of the fast subsystem tends to infinity. This results in the layered structure of P. In the left-outer region, P is given by (4.7). In the inner region, P_1 is approximated by (4.8). For P_2, we have

$$P_2(\xi) = \exp\left(\frac{-\alpha C}{\sqrt{\beta_{\mathrm{SNIC}} - \phi(\xi)}}\right)(\xi - F_1) + F_1, \quad \text{where } \phi(\xi) = \frac{\delta\xi}{1+\xi}. \tag{6.2}$$

By plugging in (6.1) into (B.4), we find that $\mathcal{F}(\beta)$ is a decreasing continuous function in the vicinity of β_{SNIC} ($\beta < \beta_{\mathrm{SNIC}}$) and $\mathcal{F}(\beta_{\mathrm{SNIC}} - 0) = F_1$. However, in contrast to the case of homoclinic bifurcation, in the present case, we have

$$\mathcal{F}'(\beta_{\mathrm{SNIC}} - 0) = 0. \tag{6.3}$$

The analyses for the fixed point of P (Sections 5.1 and 5.2) can be carried out for the case of SNIC with minor modifications. As to the bursting behavior, (6.3) implies that the size of the boundary layer (the part of the inner region where P substantially deviates from its piecewise-linear approximation) in the present case is bigger than in the case of homoclinic bifurcation. Therefore, we expect larger windows in the parameter space corresponding to irregular behavior.

6.2. Saddle-node of limit cycles

If the fast oscillations in the bursting system terminate through a SNLC bifurcation, the period of oscillations remains finite. This implies that for sufficiently small $\alpha > 0$, the inner region is absent in the description of the first return map P (see Fig. 10). Therefore, P is close to a piecewise-linear map. Under the variation of the control parameter, the superstable cycles of P exhibit reverse period-adding bifurcations as was shown in Section 5.3.

Remark 6.1.

(a) The branch of unstable periodic orbits appearing from the SNLC bifurcation may limit onto the branch of equilibria creating a homoclinic bifurcation (see Fig. 10). The latter may affect the stable periodic orbits participating in bursting causing a substantial increase in the period of oscillations. Thus, if SNLC and HC

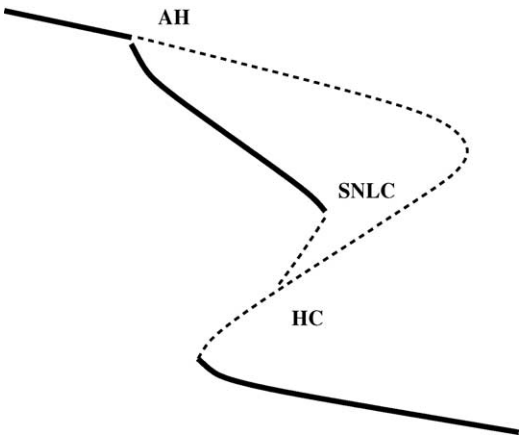

Fig. 10. An example of the bifurcation diagram for the fast subsystem (compare with Fig. 3). The stable limit cycles terminate through a SNLC bifurcation.

bifurcations are not sufficiently separated, the qualitative form of the first return map will be close to that described in the previous sections.

(b) In general, function $F(u)$ in (4.4) may not be monotone as we found for the Chay model. The convexity of $F(u)$ may result in additional fixed points in the left-outer region, thus, adding new features to the bifurcation structure of the problem. In particular, the blue-sky catastrophe in the model of a bursting neuron in [42] is consistent with the SN of equilibrium bifurcation in the left-outer region of the first return map.

6.3. Andronov–Hopf bifurcation

As in the case of the SNLC, at the AH bifurcation the period remains finite. Therefore, the remarks made for the case of SNLC above apply to the present case. We note that in this case, the analysis should take into account a possible delay in transition to the branch of slow motion due to the smallness of α [2].

Acknowledgments

The author thanks Philip Holmes and Andrey Shilnikov for helpful conversations and anonymous referees for useful suggestions. This work was partially supported by National Science Foundation Award 0417624.

Appendix A. Parameter values

The values of the parameters for the nondimensional model (2.4)–(2.6) are given in Table A.1
The steady state functions for the gating variables are given by

$$y_\infty = \frac{\alpha_y}{\alpha_y + \beta_y}, \quad y \in \{m, n, h\},$$

where

$$\alpha_m = (2.5 + v)(1 - \mathrm{e}^{-(v+2.5)})^{-1}, \qquad \beta_m = 4\mathrm{e}^{-(v+5)/1.8}, \qquad \alpha_h = 0.07\,\mathrm{e}^{-(v+5)/2},$$
$$\beta_h = (1 + \mathrm{e}^{-(v+2)})^{-1}, \qquad \alpha_n = 0.1(2 + v)(1 - \mathrm{e}^{-(v+2)}), \qquad \beta_n = 0.125\,\mathrm{e}^{-(v+3)/8}.$$

Table A.1

E_I	10
ϵ	0.1353
γ	1.833×10^{-2}
E_K	−7.5
a	1.059
δ	0.01, 0.02
E_{Ca}	10
l	4.12×10^{-3}
k_v	10
E_l	−4
ρ	1.174×10^{-2}
k_t	1/230

The time constant of the activation of the voltage-dependent K^+ channel is given by

$$\tau = (\alpha_n + \beta_n)^{-1}.$$

Appendix B. Properties of $\mathcal{F}(\beta)$

To show that $\mathcal{F}(\beta)$ has the properties listed in the beginning of Section 5, we use (4.4) to rewrite the definition of $\mathcal{F}(\beta)$:

$$\mathcal{F}(\beta) \equiv F\left(\frac{\beta}{\delta-\beta}\right) = \frac{\int_0^{\mathcal{T}(\beta)} f(v(s))\,\mathrm{e}^{\alpha(s-\mathcal{T}(\beta))}\,\mathrm{d}s}{\gamma\int_0^{\mathcal{T}(\beta)} \mathrm{e}^{\alpha(s-\mathcal{T}(\beta))}\,\mathrm{d}s} = \frac{\alpha}{\gamma}\frac{\int_0^{\mathcal{T}(\beta)} f(v(s))\,\mathrm{e}^{\alpha(s-\mathcal{T}(\beta))}\,\mathrm{d}s}{1-\mathrm{e}^{-\alpha\mathcal{T}(\beta)}}. \tag{B.1}$$

We split the integral in the nominator into two integrals over $[0, T_0]$ and $[T_0, \mathcal{T}(\beta)]$ and use (3.4) to obtain

$$\frac{1}{\gamma}\int_0^{\mathcal{T}(\beta)} f(v(s))\,\mathrm{e}^{\alpha(s-\mathcal{T}(\beta))}\,\mathrm{d}s = \frac{1}{\gamma}\int_0^{T_0} f(v(s))\,\mathrm{e}^{\alpha(s-T_0)}\,\mathrm{e}^{\alpha(T_0-\mathcal{T}(\beta))}\,\mathrm{d}s$$
$$+\frac{1}{\gamma}\int_{T_0}^{\mathcal{T}(\beta)} f(v(s))\,\mathrm{e}^{\alpha(s-\mathcal{T}(\beta))}\,\mathrm{d}s \approx F_0 T_0\,\mathrm{e}^{-\alpha(\mathcal{T}(\beta)-T_0)} \tag{B.2}$$

$$+\alpha^{-1}F_1(1-\mathrm{e}^{-\alpha(\mathcal{T}(\beta)-T_0)}), \tag{B.3}$$

where F_0 and F_1 are defined in (4.8) and (4.13), respectively. Thus,

$$\mathcal{F}(\beta) = \alpha F_0 T_0 \frac{\mathrm{e}^{-\alpha(\mathcal{T}(\beta)-T_0)}}{1-\mathrm{e}^{-\alpha\mathcal{T}(\beta)}} + F_1\frac{1-\mathrm{e}^{-\alpha(\mathcal{T}(\beta)-T_0)}}{1-\mathrm{e}^{-\alpha\mathcal{T}(\beta)}} + \text{h.o.t.}. \tag{B.4}$$

By differentiating $\mathcal{F}$, we find the leading order term in the expansion of $\mathcal{F}'(\beta)$ for $\beta \to \beta_{\mathrm{HC}} - 0$:

$$\mathcal{F}'(\beta) = \alpha^2 T'(\beta)\,\mathrm{e}^{-\alpha(\mathcal{T}(\beta)-T_0)}\frac{(F_1 - F_0 + \mathrm{O}(\alpha))T_0}{(1-\mathrm{e}^{-\alpha\mathcal{T}(\beta)})^2} + \text{h.o.t.}. \tag{B.5}$$

By combining (B.5) and (3.4), we arrive at

$$\mathcal{F}'(\beta) = \frac{\alpha^2\mu d^{\alpha\mu}(F_1 - F_0 + \mathrm{O}(\alpha))T_0}{(\beta_{\mathrm{HC}}-\beta)^{1-\alpha\mu}(1-\mathrm{e}^{-\alpha\mathcal{T}(\beta)})^2} + \text{h.o.t.}. \tag{B.6}$$

The asymptotic formulas (B.4)–(B.6) and Statement (C1) of Section 3 imply the properties of $\mathcal{F}(\beta)$ stated in Section 5.

References

[1] J.C. Alexander, D.-Y. Cai, On the dynamics of bursting systems, J. Math. Biol. 29 (1991) 405–423.
[2] V.I. Arnold, V.S. Afroimovich, Y.S. Ilyashenko, L.P. Shilnikov, Dynamical Systems, vol. V, Springer-Verlag, 1994.
[3] V.N. Belykh, I.V. Belykh, M. Colding-Jorgensen, E. Mosekilde, Homoclinic bifurcations leading to the emergence of bursting oscillations in cell models, Eur. Phys. J. E 3 (2000) 205–219.
[4] N.N. Bogoliubov, Yu.A. Mitropolsky, Asymptotic Methods in the Theory of Non-linear Oscillations, Hindustan Publishing Corp., Delhi, 1961.
[5] R.J. Butera, J. Rinzel, J.C. Smith, Models of respiratory rhythm generation in the pre-Botzinger complex. I. Bursting pacemaker neurons, J. Neurophysiol. 82 (1999) 382–397.
[6] T.R. Chay, Chaos in a three-variable model of an excitable cell, Physica D 16 (1984) 233–242.
[7] T.R. Chay, Y.S. Fan, Y.S. Lee, Bursting, spiking, fractals, and universality in biological rhythms, Int. J. Bifurc. Chaos 5 (3) (1995) 595–635.
[8] T.R. Chay, J. Keizer, Minimal model for membrane oscillations in the pancreatic β-cell, Biophys. J. 42 (1983) 181–190.
[9] T.R. Chay, J. Rinzel, Bursting, beating, and chaos in an excitable membrane model, Biophys. J. 47 (1985) 357–366.
[10] P. Dayan, L.F. Abbot, Theoretical Neuroscience: Computational and Mathematical Theory of Neural Systems, MIT Press, Cambridge, MA, 2001.
[11] B. Ermentrout, Simulating, Analyzing, and Animating Dynamical Systems: A Guide to XPPAUT for Researches and Students, SIAM, Philadelphia, 2002.
[12] G.B. Ermentrout, N. Kopell, Parabolic bursting in an excitable system coupled with a slow oscillation, SIAM J. Appl. Math. 46 (1986) 233–253.
[13] R. Ghigliazza, P. Holmes, Minimal models of bursting neurons: the effects of multiple currents, conductances and timescales, Preprint, 2004.
[14] R. Ghigliazza, P. Holmes, A minimal model of a central pattern generator for insect locomotion, Preprint, 2004.
[15] J. Guckenheimer, R. Harris-Warrick, J. Peck, A. Willms, Bifurcation, bursting, and spike-frequency adaptation, J. Comp. Neurosci. 4 (1997) 257–277.
[16] J. Guckenheimer, P. Holmes, Nonlinear Oscillations, Dynamical Systems, and Bifurcations of Vector Fields, Springer, 1983.
[17] J.L. Hindmarsh, R.M. Rose, A model of neuronal bursting using three coupled first order differential equations, Proc. R. Soc. London B 221 (1984) 87–102.
[18] A.L. Hodgkin, A.F. Huxley, A quantitative description of membrane current and its application to conduction and excitation in nerve, J. Physiol. 117 (1952) 500–544.
[19] F.C. Hoppensteadt, E.M. Izhikevich, Weakly connected neural networks, Applied Mathematical Sciences, vol. 126, Springer-Verlag, 1997.
[20] E.M. Izhikevich, Neural excitability, spiking, and bursting, Int. J. Bifurc. Chaos 10 (2000) 1171–1266.
[21] C.K.R.T. Jones, Geometric singular perturbation theory, in: CIME Lectures in Dynamical Systems, Lecture Notes in Mathematics, Springer-Verlag, 1994.
[22] T. Kiemel, P.J. Holmes, A model for the periodic synaptic inhibition of a neuronal oscillator, IMA J. Math. Appl. Biol. Med. 4 (1987) 145–169.
[23] M. Krupa, P. Szmolyan, Relaxation oscillation and canard explosion, JDE 174 (2001) 312–368.
[24] A.Yu. Kuznetsov, Elements of Applied Bifurcation Theory, Springer, 1998.
[25] M. Levi, A period-adding phenomenon, SIAM J. Appl. Math. 50 (4) (1990) 943–955.
[26] T. LoFaro, N. Kopell, Timing regulation in a network reduced from voltage-gated equations to a one-dimensional map, J. Math. Biol. 38 (1999) 479–533.
[27] G.S. Medvedev, J.E. Cisternas, Multimodal regimes in a compartmental model of the dopamine neuron, Physica D 194 (2004) 333–356.
[28] A. Milik, P. Szmolyan, H. Løffelman, E. Grøller, Geometry of mixed-mode oscillations in the 3D autocatalator, Int. J. Bifurc. Chaos 8 (1998) 505–519.
[29] E.F. Mishchenko, Yu.S. Kolesov, A.Yu. Kolesov, N.Kh. Rozov, Asymptotic Methods in Singularly Perturbed Systems, Consultants Bureau, New York, 1994.
[30] E. Mosekilde, B. Lading, S. Yanchuk, Yu. Maistrenko, Bifurcation structure of a model of bursting pancreatic cell, BioSystems 63 (2001) 3–13.
[31] M. Pernarowski, R. Miura, J. Kevorkian, Perturbation techniques for models of bursting electrical activity in the pancreatic beta cells, SIAM J. Appl. Math. 52 (1992) 1627–1650.
[32] P.F. Pinsky, J. Rinzel, Intrinsic and network rhythmogenesis in a reduced Traub model for CA3 neurons, J. Comp. Neurosci. 1 (1994) 39–60.

[33] J. Rinzel, A formal classification of bursting mechanisms in excitable systems, in: A.M. Gleason (Ed.), Proceedings of the International Congress of Mathematicians, AMS, 1987, pp. 135–169.
[34] J. Rinzel, G.B. Ermentrout, Analysis of neural excitability and oscillations, in: C. Koch, I. Segev (Eds.), Methods in Neuronal Modeling, MIT Press, Cambridge, MA, 1989.
[35] J. Rinzel, W.C. Troy, A one-variable map analysis of bursting in the Belousov–Zhabotinskii reaction, in: J.A. Smoller (Ed.), Nonlinear Partial Differential Equations, AMS, Providence, 1882, pp. 411–427.
[36] J. Rinzel, W.C. Troy, Bursting phenomena in a simplified Oregonator flow system model, J. Chem. Phys. 76 (1982) 1775–1789.
[37] M.E. Rush, J. Rinzel, Analysis of bursting in a thalamic neuron model, Biol. Cybernet. 71 (1994) 281–291.
[38] A.N. Sharkovski, Yu.L. Maistrenko, E.Yu. Romanenko, Difference Equations and their Applications, Kluwer Academic Publishers Group, 1993.
[39] A.S. Sherman, Calcium and membrane potential oscillations in pancreatic β-cells, in: H.G. Othmer, F.R. Adler, M.A. Lewis, J.C. Dallon (Eds.), Case Studies in Mathematical Modeling — Ecology, Physiology and Cell Biology, Prentice-Hall, 1996.
[40] A.S. Sherman, Y.-X. Li, J. Keizer, Whole cell models, in: C.P. Fall, E.S. Marland, J.M. Wagner, J.J. Tyson (Eds.), Computational Cell Biology, Springer, 2000.
[41] A.S. Sherman, J. Rinzel, J. Keizer, Emergence of organized bursting in clusters of pancreatic β-cells by channel sharing, Biophys. J. 54 (1988) 411–425.
[42] A. Shilnikov, G. Cymbalyuk, Transition between tonic-spiking and bursting in a neuron model via the blue-sky catastrophe, Preprint, 2004.
[43] A. Shilnikov, R.L. Calabrese, G. Cymbalyuk, Mechanism of bi-stability: tonic spiking and bursting in a neuron model, Preprint, 2004.
[44] F. Takens, Transition from periodic to strange attractors in constrained equations, in: Dynamical Systems, Bifurcation Theory, Longman, 1987.
[45] D. Terman, Chaotic spikes arising from a model of bursting in excitable membranes, SIAM J. Appl. Math. 51 (1991) 1418–1450.
[46] D. Terman, The transition from bursting to continuous spiking in excitable membrane models, J. Nonlinear Sci. 2 (1992) 135–182.
[47] X.-J. Wang, Calcium coding and adaptive temporal computation in cortical pyramidal neurons, J. Neurophysiol. 79 (1998) 1549–1566.
[48] X.-J. Wang, Fast burst firing and short-term synaptic plasticity: a model of neocortical chattering neurons, Neuroscience 89 (1999) 347–362.
[49] X.-J. Wang, J. Rinzel, Oscillatory and bursting properties of neurons, in: M.A. Arbib (Ed.), Handbook of Brain Theory and Neural Networks, MIT Press, Cambridge, MA, 1995, pp. 689–691.
[50] S. Wiggins, Global Bifurcations and Chaos, Springer-Verlag, 1988.
[51] D. de Vries, Multiple bifurcations in a polynomial model of bursting oscillations, J. Nonlinear Sci. 8 (1998) 281–316.
[52] S. Yoshizava, H. Osada, J. Nagumo, Pulse sequences generated by a degenerate analog neuron model, Biol. Cybernet. (1982) 45.